BIOCHEMISTRY
including biophysical chemistry & molecular biology

Accelerated Publication

pubs.acs.org/biochemistry

Variations in Protein–Flavin Hydrogen Bonding in a Light, Oxygen, Voltage Domain Produce Non-Arrhenius Kinetics of Adduct Decay

Brian D. Zoltowski, Abigail I. Nash, and Kevin H. Gardner*

Department of Biochemistry, University of Texas Southwestern Medical Center, Dallas, Texas 75390-8816, United States

Supporting Information

ABSTRACT: Light, oxygen, voltage (LOV) domains utilize a conserved blue light-dependent mechanism to control a diverse array of effector domains in biological and engineered proteins. Variations in the kinetics and efficiency of LOV photochemistry fine-tune various aspects of the photic response. Characterization of the kinetics of a key aspect of this photochemical mechanism in EL222, a blue light responsive DNA binding protein from *Erythrobacter litoralis* HTCC2594, reveals unique non-Arrhenius behavior in the rate of dark-state cleavage of the photochemically generated adduct. Sequence analysis and mutagenesis studies establish that this effect stems from a Gln to Ala mutation unique to EL222 and homologous proteins from marine bacteria. Kinetic and spectroscopic analyses reveal that hydrogen bonding interactions between the FMN N1, O2, and ribityl hydroxyls and the surrounding protein regulate photocycle kinetics and stabilize the LOV active site from temperature-induced alteration in local structure. Substitution of residues interacting with the N1–O2 locus modulates adduct stability, structural flexibility, and sequestration of the active site from bulk solvent without perturbation of light-activated DNA binding. Together, these variants link non-Arrhenius behavior to specific alteration of an H-bonding network, while affording tunability of photocycle kinetics.

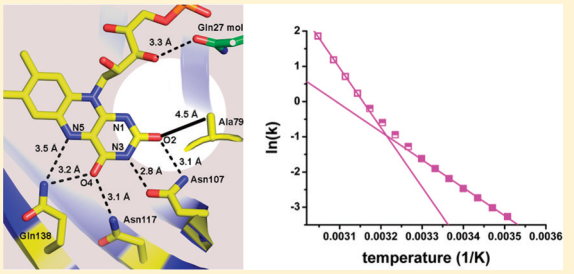

The ability of light, oxygen, voltage (LOV) domains to couple environmental stimuli to alterations in cellular signaling has led to the development of bioengineered tools for manipulating biological pathways in vitro and in vivo.[1−5] These systems use a conserved signaling mechanism based on blue light-dependent formation of a covalent cysteine–flavin adduct.[6] Bond formation is coupled to reorientation of protein elements adjacent to the LOV domain, regulating their participation in protein–protein interactions or modulating the activity of kinases, phosphodiesterases, DNA binding, or other diverse effector families.[6−11] Recently, it has been demonstrated that LOV domains can be engineered to confer light-dependent control to non-photosensitive enzymes (e.g., histidine kinase[5] and GTPase[3]) and DNA binding proteins.[2] The utility of both native and engineered LOV proteins has spurred interest in characterizing and manipulating their basic photochemical mechanisms, including regulation of photocycle kinetics and signal transduction.[6,12−15]

Studies that have generated LOV variants with altered photocycle kinetics can largely be divided into two camps: those that have mutated conserved residues in or near the flavin-binding pocket (e.g., the adduct-forming active site Cys)[12,16−18] and those that have identified naturally varying residues that direct the diverse range of photocycle kinetics observed in natural systems.[15,19,20] Whereas the former method has provided keen insight into the biophysics of adduct formation,[12,21,22] as well as the development of in vivo tools,[1] these variants can alter the signaling mechanism of LOV domains.[12,18] Alternatively, the latter strategy has identified naturally occurring residue selections that can regulate adduct stability with minimal effects on the signaling mechanism.[15]

Mutational analyses of conserved residues within LOV domains have revealed mechanisms of adduct formation, regulation of adduct formation kinetics and yield, and factors regulating adduct stability. For instance, initial studies of photocycle-altering variants focused on the conserved Cys moiety that is directly involved in adduct formation. Time-resolved UV–visible absorbance and EPR measurements demonstrated rapid formation of a flavin triplet state that readily formed a radical intermediate in Cys → Ala and Cys → Ser variants.[21,22] In addition, random mutagenesis that aimed to identify rapid cycling phenotypes indicated that steric interactions with the active site Cys can appreciably affect the rate of adduct decay.[16] Complementary targeted mutation of conserved active site residues confirmed the importance of Cys and flavin steric contacts,[13,17,18] H-bonding interactions within the flavin core,[12] and the access of solvent and gas to the active site as a means of kinetic control.[17] While these variants can tune adduct lifetime over 2 orders of magnitude, they can also destabilize flavin binding and alter signaling pathways.[12,18]

In parallel with this approach, detailed analyses of naturally occurring variants have identified sites that tune adduct-state lifetime over 4 orders of magnitude with minimal effects on the photochemical mechanism.[15] In addition to steric effects at the

Received: June 24, 2011
Revised: September 15, 2011
Published: September 16, 2011

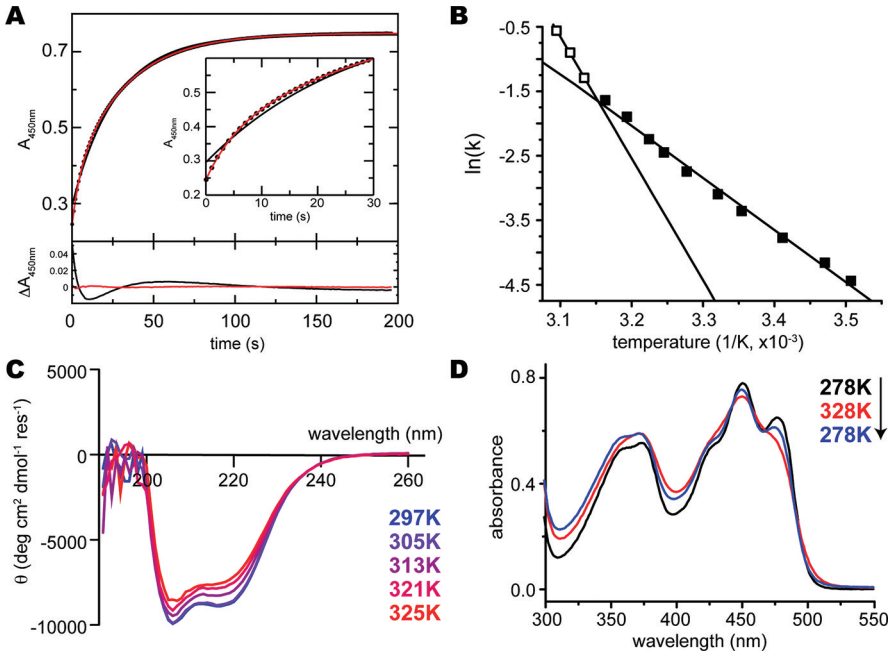

Figure 1. Effects of temperature on EL222 dark-state recovery kinetics and structure. (A) Dark-state recovery kinetics of WT EL222 (14−222) at 297 K as monitored by increased absorbance at 450 nm postillumination. We noted that these recovery curves can be fit by either monoexponential (black) or biexponential curves (red), with some data sets fitting slightly better to biexponential curves at initial time points [insets show both initial recovery points and residuals (additional discussion in the Supporting Information)]. (B) Non-Arrhenius behavior of dark-state recovery of WT EL222 (14−222). At low temperatures (<318 K), Arrhenius behavior is observed with an E_a of 63 kJ/mol; at approximately 318 K, we observed a transition to a second linear regime with a higher E_a of 115 kJ/mol. (C) Circular dichroism spectra of EL222 as a function of temperature. The shape of the CD spectra is temperature-independent; the minor loss of intensity reflects precipitation at high temperatures. (D) At 328 K, a noticeable loss of vibronic structure in the FMN absorbance is noted (red) compared to that of WT at 278 K (black). Incubation at 278 K for 10 min (including cooling time) results in the partial return of vibronic structure (blue).

active site Cys, this study demonstrated that the primary mechanisms mediating diverse LOV adduct-state decay kinetics include electronic and steric alteration of the flavin reduction potential and the access of solvent to the active site. Notably, crystallographic studies of these variants revealed no alteration in protein structure or function despite the significant alteration in photocycle kinetics. Similarly, comparisons of the sequences of two homologous bacterial LOV proteins with distinct photocycle kinetics identified a key Arg residue interacting with the ribityl backbone that dictates a fast or slow cycling phenotype.[19] This study demonstrated that changes to elements outside of the LOV domain can have >100-fold effects on photocycle kinetics as well, potentially by allosteric modification of LOV structure.

Importantly, studies of diverse LOV proteins suggest that their photocycle kinetics may be perturbed by structural changes in the surrounding protein. Initial studies of plant phototropin LOV1 and LOV2 domains revealed distinct differences in cycling kinetics, with LOV1 domains generally having longer-lived adducts than their LOV2 counterparts.[20] FTIR, circular dichroism (CD), and NMR experiments indicate that LOV2 domains undergo a partial disordering of local structure following photoexcitation,[20,23−25] whereas LOV1 domains do not exhibit the same flexibility. These differences have primarily been attributed to a single residue on the *re* face of the flavin, which differs between LOV1 (Leu) and LOV2 (Phe).[20] Similarly, laser-induced optoacoustic spectroscopy (LIOAS) data revealed that mutations that alter photocycle kinetics and yield can also change the magnitude of light-dependent volume changes.[12] However, the role of conformational fluctuations in mediating adduct-state stability is still largely unknown.

We have obtained some insight into these issues with our studies of bacterial LOV−HTH (LOV−helix−turn−helix) protein EL222.[26] Identified in the marine bacterium *Erythrobacter litoralis* HTCC2594, this protein contains a photosensitive LOV domain and a DNA-binding HTH domain effector. Structural and functional characterization of EL222 established that photochemical changes within the EL222 LOV domain lead to separation of the LOV and HTH domains and subsequent light-induced DNA binding.[26] Herein, we characterize the kinetics of adduct cleavage in EL222 and identify a new natural LOV variant that alters the lifetime of the photoinduced Cys−flavin adduct, while maintaining the native protein conformation and signaling mechanisms. Moreover, we demonstrate unique non-Arrhenius behavior indicating temperature-dependent conformational fluctuations that also affect adduct stability.

MATERIALS AND METHODS

Cloning and Protein Purification. Rate-altering variants were produced using the QuikChange protocol (Stratagene) within the context of an N-terminally truncated LOV−HTH construct of EL222 (14−222) with an N-terminal His_6 tag.[26] Mutations were verified by DNA sequencing (University of Texas Southwestern Sequencing Facility). All LOV−HTH (14−222) and LOV only (14−144) EL222 variants were expressed in *Escherichia coli* BL21(DE3) cells. Cells were induced with 0.1 mM isopropyl thiogalactoside (IPTG) for 22 h at 18 °C. Cells were harvested, pelleted, and stored in 100 mM NaCl and 50 mM Tris (pH 8.0).

Table 1. Kinetic and Thermodynamic Parameters for EL222 Dark-State Reversion[a]

	rate (s^{-1})	τ (s)	E_a (kJ/mol)	$\Delta H^{\ddagger}$ (kJ/mol)	$\Delta S^{\ddagger}$ (kJ/mol, 318 K)
WT (14–222)	0.034	29	63 ± 2, **115 ± 4**[c]	61 ± 3, **107 ± 5**	−22 ± 10, **26 ± 10**
WT (14–144)[b]	0.045	22	75	72	−9.1
A79Q (14–222)	0.0044	227	100, **138**	97, **135**	12, **51**
A79R (14–222)	0.37	2.7	64, **108**	63, **109**	−13, **56**
A79T (14–222)[d]	0.11	8.9	68, **141**	70, **124**	−11, **39**

[a]Kinetic parameters (rate and τ) were measured at 298 K, while thermodynamic parameters (E_a, $\Delta H^{\ddagger}$, and $\Delta S^{\ddagger}$) were determined by fits to eight temperature points (285–308 K) for the low-temperature regime and the four highest temperature points (319–328 K) for the high-temperature regime (bold). [b]WT (14–144) shows only linear Arrhenius behavior, so only one set of thermodynamic parameters is reported. [c]Error reported as the standard deviation of the mean for three independent measurements (Materials and Methods), which we assume to be applicable to all data sets given similar data quality among all. [d]Thermodynamic parameters for A79T at high temperatures may be imprecise because of difficulties in fitting the curved Arrhenius and Eyring plots exhibited by this variant.

Proteins were purified by Ni-NTA chromatography at 4 °C with gradient elution from 10 to 500 mM imidazole in 100 mM NaCl and 50 mM Tris (pH 8.0). The His_6 tag was removed via incubation with His_6-tagged TEV protease[27] overnight at 4 °C. An additional round of Ni-NTA chromatography was conducted to remove His_6-TEV and the His_6 tag. EL222 samples were then subjected to Superdex S75 size-exclusion chromatography with 100 mM NaCl and 50 mM Tris (pH 8.0) for all subsequent analysis.

UV–Visible Absorbance Spectroscopy and Kinetics. UV–visible absorbance spectroscopy of EL222 variants was conducted on a Varian Cary 50 spectrophotometer. Protein samples were kept at a concentration of approximately 40 μM and measured using a 1 cm path length cuvette at temperatures between 285 and 328 K.

Kinetics measurements of EL222 dark-state recovery were obtained by measuring the absorbance at 450 nm after excitation with a camera flash. Absorbance measurements were taken at a sampling frequency varied to provide approximately 30 measurements per half-life, ensuring sufficient data coverage while not continuously illuminating the sample. Solvent isotope effect (SIE = k_{H_2O}/k_{D_2O}) measurements were taken similarly, using a 99% D_2O-containing form of the buffer.

We evaluated both mono- and biexponential fitting to extract kinetic parameters from these decays. While monoexponential fitting adequately modeled most decays [$\tau \sim 31$ s at 298 K (Figure 1A and Figure S1 and Table S1 of the Supporting Information)], we noted nonrandom residuals at the beginning of some recoveries that suggested a minor fast component might be present. Biexponential fitting revealed these two processes ($\tau \sim 28$ and 4.7 s at 298 K), with significant sample-to-sample variation in amplitude between 5 and 20% of the recovery. Coupling this variation with instrumental limitations on sampling rate that complicate precisely fitting this faster process at high temperatures, we opted to use monoexponential fitting to determine rate (k) and time constants ($1/k$) from our kinetic data. Critically, comparisons of Arrhenius plots of the rates extracted from both approaches showed the same non-Arrhenius behavior for rates from monoexponential fits and the slow component of the biexponential fits (Figure S1 of the Supporting Information), establishing the validity of this approach. Additional commentary on this point is provided in the Supporting Information.

To estimate errors in parameters extracted from Arrhenius and Eyring analyses, we recorded kinetic data from each of three separate samples of WT EL222 (14–222), independently calculating thermodynamic parameters from each of these data sets. Averages and standard deviations of the mean were calculated for E_a, $\Delta H^{\ddagger}$, and $\Delta S^{\ddagger}$ for these data (Table 1). Analyses of other proteins were acquired from single samples, which we assume to have errors comparable to those of WT EL222 (14–222) given comparable data quality.

CD Spectroscopy. CD spectroscopy measurements of EL222 variants were taken using an Aviv model 62DS spectrometer. Samples were incubated for 10 min at the stated temperatures prior to data collection. Spectra were obtained between 260 and 190 nm in 1 nm steps, with 3 s signal averaging at every wavelength. Spectra were corrected for buffer and averaged over three scans.

Nuclear Magnetic Resonance. Solution ^{15}N–^{1}H HSQC spectra[28] were recorded on 200–300 μM samples on a Varian 800 MHz spectrometer equipped with a cryogenically cooled, triple-resonance probe, with samples at 298 K. Light-state samples were collected as described previously.[26] All data were processed using NMRPipe[29] and analyzed using NMRViewJ.[30]

RESULTS

EL222 exhibits a typical LOV domain photocycle[26] with the photochemical formation of a cysteinyl–flavin C4a adduct leading to a significant decrease in visible absorbance above 400 nm. Once illumination had ceased, the adduct spontaneously decays with a time constant of approximately 30 s at 298 K that we observed with either mono- or biexponential fitting of the kinetic traces (Figure 1A, Table 1, and Table S1 of the Supporting Information). We observed a fast component in biexponential fits of certain traces ($\tau \sim 4.7$ s at 298 K in Figure 1A), but this minor component varied by sample between 5 and 20% of the total recovery amplitude and was difficult to precisely characterize at high temperatures. As such, we conducted all further analyses using monoexponential fitting. Analysis of the temperature dependence of the dark-state recovery kinetics revealed unusual non-Arrhenius behavior, with two distinct states exhibiting different linear Arrhenius dependencies (Figure 1B and Table 1). As such, the two regimes differ in their relative activation barriers and corresponding entropic and enthalpic contributions to adduct stability. Below 318 K, EL222 displays an activation barrier of 63 ± 2 kJ/mol. Above 318 K, we observed an abrupt transition to a second linear regime with a 1.8-fold elevated activation energy of 115 ± 4 kJ/mol (Figure 1B and Table 1). Eyring plot analysis reveals that the two regions differ in their enthalpic and entropic contributions (Table 1), with a more favorable entropy of activation in the high-temperature regime (26 ± 10 kJ/mol) than in the low-temperature regime (−21 ± 10 kJ/mol at 318 K).

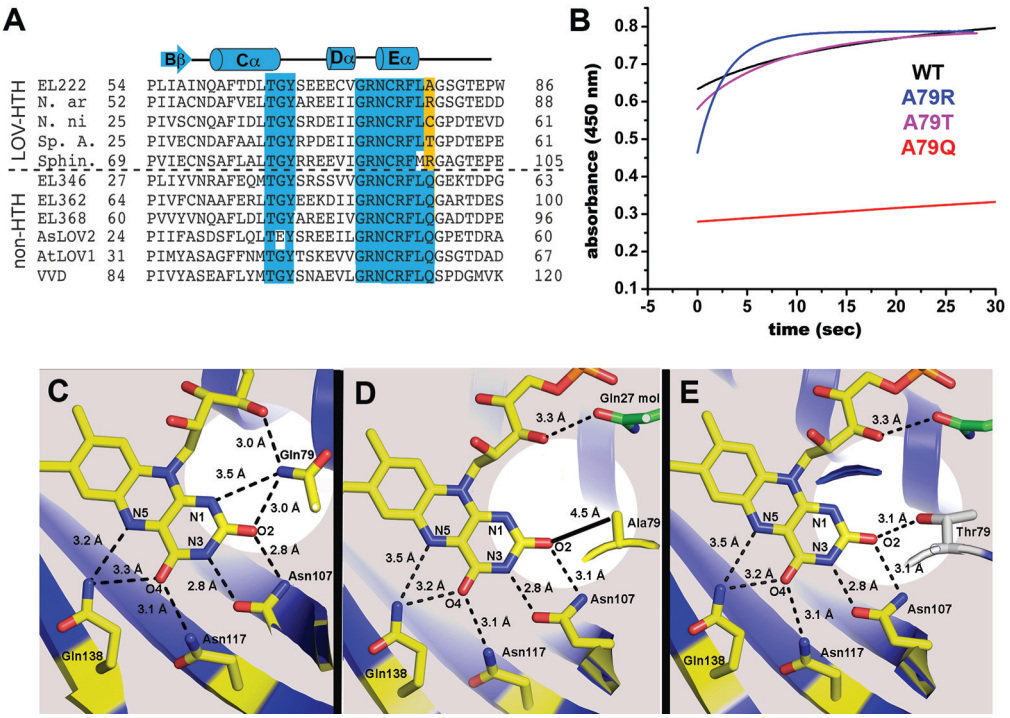

Figure 2. Structural and functional effects of natural sequence variants at the A79 position. (A) Conserved LOV residues (blue) include variations at a conserved glutamine residue as seen in five LOV−HTH proteins (above the dashed line) from *Erythrobacter litoralis* (EL222), *Novosphingobium aromaticivorans* Saro_1231 (N. ar), *Novosphingobium nitrogenifigens* (N. ni), *Sphingopyxis alaskensis* Sala_1000 (Sp A.), and *Sphingomonas* (Sphin); these are aligned with LOV domains from selected proteins without HTH domains (below the dashed line), including the three other *E. litoralis* LOV proteins (EL346, EL362, and EL368), *Avena sativa* phototropin 1 LOV2 (AsLOV2), *Arabidopsis thaliana* phototropin 1 LOV1 (AtLOV1), and *Neurospora* Vivid (VVD) A conserved GRNCRFLQ motif is altered in five bacterial LOV−HTH proteins (orange). (B) Kinetic traces of adduct cleavage postillumination as monitored by absorbance at 450 nm and 298 K, with all curves normalized to the same asymptotic A_{450}. Two variants accelerate the rate of adduct decay (A79R and A79T) compared to the wild type, while A79Q stabilizes the adduct. (C) The conserved Gln residue in most LOV domains forms an H-bonding network (highlighted with the white circle) with groups on the FMN ring and ribityl chain (Gln79 interacting with ring N1 and O2, plus a ribityl hydroxyl as seen in VVD).[10] (D) Ala79 in EL222 cannot form H-bonds to either N1 or O2.[26] Note that Gln27 from another molecule in the crystallographic unit forms an H-bond to the backbone hydroxyl. (E) Modeling suggests that artificial introduction of a Thr at position 79 in EL222 (gray) can H-bond to O2, but not the N1 or backbone hydroxyl groups.

While LOV domains typically exhibit linear Arrhenius behavior for the temperature dependence of adduct scission,[12] nonlinear Arrhenius behavior has occasionally been observed in biochemical and chemical systems. This can range from curved Arrhenius behavior, as seen in the decay of the pB signaling state in photoactive yellow protein,[31] to abrupt transitions between two linear Arrhenius regimes, as occasionally observed in a variety of enzymes.[32] These are often interpreted as involving a structural transition that alters or inactivates the catalytic mechanism. While these transitions most commonly link a higher-activity state at low temperatures with a lower-activity high-temperature state, we strikingly observed that adduct scission in EL222 occurred more rapidly at high temperatures than expected from low-temperature data. We suggest that structural or mechanistic perturbation of LOV chemistry in EL222 could stem from a variety of sources, including disruption of the FMN binding pocket via local alteration of secondary structure or a global dislocation of the HTH domain from the LOV core (which may alter the LOV β-sheet, immediately adjacent to the flavin itself).

Solvent isotope effect (SIE) experiments were conducted to determine whether there is a change in the adduct scission mechanism at high temperatures. Interestingly, EL222 displays a high SIE of approximately 4 between 285 and 328 K (Figure S2 of the Supporting Information). The temperature independence of the SIE suggests that abstraction of a proton from N5 is rate-limiting[15,16] at all temperatures, eliminating the LOV mechanism as the source of the non-Arrhenius behavior. Rather, the unusual break in the linear Arrhenius dependency likely results from temperature-dependent structural perturbation.

To evaluate the role of the HTH domain in the non-Arrhenius behavior of EL222, we examined the temperature dependence of the kinetics of adduct scission in the isolated LOV domain [residues 14−144, compared to the LOV−HTH (14−222) construct]. We observed only one linear regime in the isolated LOV domain (Figure S3 of the Supporting Information), but we note that the construct irreversibly aggregates above 318 K, preventing data collection at these higher temperatures. The truncated protein also demonstrated a minor alteration in the energetics of adduct scission with an 8 kJ/mol higher energy of activation compared to that of a LOV−HTH construct (Table 1). The increase in the energy of activation is offset by a more favorable entropy of activation (−9.1 kJ/mol at 298 K). The minor elevation of the activation barrier may indicate that, whereas the HTH domain stabilizes the solubility of EL222 at elevated temperatures, it may slightly destabilize the light-state adduct. Thus, we must consider the effect of alteration in local structure on the non-Arrhenius behavior.

To test this possibility, we used CD and UV−visible absorbance spectra as probes of secondary structure and local

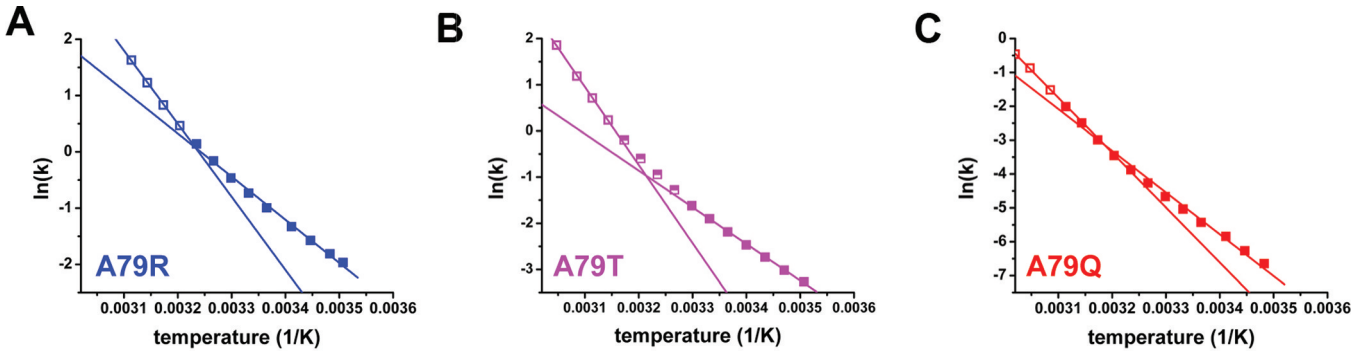

Figure 3. Effect of A79 variants on non-Arrhenius behavior in adduct scission rates. (A) The A79R variant retains non-Arrhenius behavior similar to that of WT with a stronger temperature dependence at high temperatures. Empty and filled symbols show data assigned to the high- and low-temperature regimes, respectively, with lines obtained by linear least-squares fitting to the four highest and lowest temperatures. (B) The A79T variant has non-Arrhenius behavior with a more gradual transition compared to that seen in WT and A79R, indicative of a mixed population of the two states at intermediate temperatures (half-filled symbols). (C) A79Q exhibits an only minor deviation from typical Arrhenius behavior, even up to 331 K.

flavin environment. Near-UV CD spectra of dark-state EL222 indicated a limited change in the local secondary structure at temperatures between 297 and 325 K (Figure 1C). Notably, we observed some loss of signal at elevated temperatures, consistent with minor aggregation observed in UV−visible absorbance spectra above 321 K. Notably, UV−visible absorbance spectra also identified a partially reversible loss of FMN vibronic structure above 318 K (Figure 1D). The decrease in the level of vibronic structure and the lack of secondary structure changes are consistent with an increase in the plasticity of the active site that may be coupled to enhanced solvent access at increased temperatures. Our data further indicate that most, but not all, protein in these samples recovers sufficiently to rebind FMN after such heat treatment, but we have not investigated this in detail.

Role of Active Site Residues in Modulating Non-Arrhenius Behavior. To the best of our knowledge, non-Arrhenius behavior of LOV photocycle kinetics has not previously been reported, leading us to compare the EL222 sequence to other LOV domains to look for possible contributors. We found that the terminal Gln residue found in the canonical LOV active site sequence (GRNCRFLQ[33]) is changed in EL222 to an Ala (GRNCRFL**A**) at position A79 in EL222. Examination of other LOV sequences indicated that mutations at the conserved Gln position are unique to EL222 and closely related LOV−HTH homologues from other marine bacteria (Figure 2A), showing that this site can accommodate Arg, Thr, and Cys replacements. Notably, this is specific to the LOV−HTH proteins, as other LOV domains from the same bacteria contain the canonical Gln residue.

Examination of the structures of EL222 and other LOV domains reveals that these substitutions alter hydrogen bonding interactions between the protein and the N1 and O2 positions on the isoalloxazine ring (Figure 2C−E). Specifically, the terminal Gln residue hydrogen bonds with multiple positions on the isoalloxazine ring (3.5 Å from Gln Nε to FMN N1 and 3.0 Å from Gln Ne to FMN O2 as observed in VVD[10]) with an additional interaction to the FMN O4′ ribityl hydroxyl group (3.0 Å) (Figure 2C). The naturally occurring Ala in EL222 both removes hydrogen bonding groups at this position and truncates the side chain, potentially enhancing the access of solvent to the flavin chromophore [4.5 Å from Ala Cβ to FMN O2 (Figure 2D)]. In contrast, models of an A79T substitution in EL222 suggest that it could form a Thr Oγ1−FMN O2 H-bond [~3.1 Å (Figure 2E)]; however, this would be unable to interact with N1 or O4. Similar models of an A79R mutation suggest that the longer Arg side chain could be capable of interacting with either O2 or N1, but this would require significant alteration of the local structure to prevent steric clashes with the FMN ribityl side chain. These naturally occurring variants provide an opportunity to probe the effects of H-bonding interactions at the N1 and O2 positions of the flavin ring and to evaluate the effect of mutation of the canonical Gln residue on the structure, function, and photocycle kinetics.

By making these A79 variants in EL222 and characterizing aspects of their photocycle, we found that this position substantially influences the LOV photocycle in a residue-dependent manner that depends on side chain H-bonding capabilities (Figure 2). Restoring the canonical Gln residue decreases the rate of adduct scission 10-fold (Table 1), while maintaining structure and function consistent with WT protein (Figure 2C and Figure S1 of the Supporting Information) as indicated by solution NMR spectra and electromobility shift assay (EMSA) analyses of the WT and A79Q proteins. Conversely, A79R and A79T variants increased the rate of adduct scission, with the positively charged A79R variant (τ = 2.7 s) undergoing dark reversion faster than the neutral A79T variant (τ = 8.9 s) (Table 1). Moreover, similar to WT EL222, all A79 variants exhibited non-Arrhenius behavior with two regimes differing in thermodynamic properties (Figure 3 and Table 1), but with markedly different changes in the height of activation barriers and transition temperature variations depending on the A79 substitution.

Among the variants surveyed, A79T demonstrated the largest discrepancy in activation energies between the two structural states, with a 141 kJ/mol activation energy above 318 K versus a value of 68 kJ/mol at lower temperatures (Table 1). Conversely, the long-lived A79Q variant had the smallest difference between the two states (E_a values of 138 and 99.5 kJ/mol), complicating observation of the transition between the two states somewhere above 321 K in this protein. Interestingly, the A79T variant also has non-Arrhenius behavior, with a very gradual transition between the two states in contrast with the abrupt change seen in A79R and WT EL222 (Figure 3). In this regard, A79T likely exists as a mixture of the two states, whose equilibrium population is dictated by

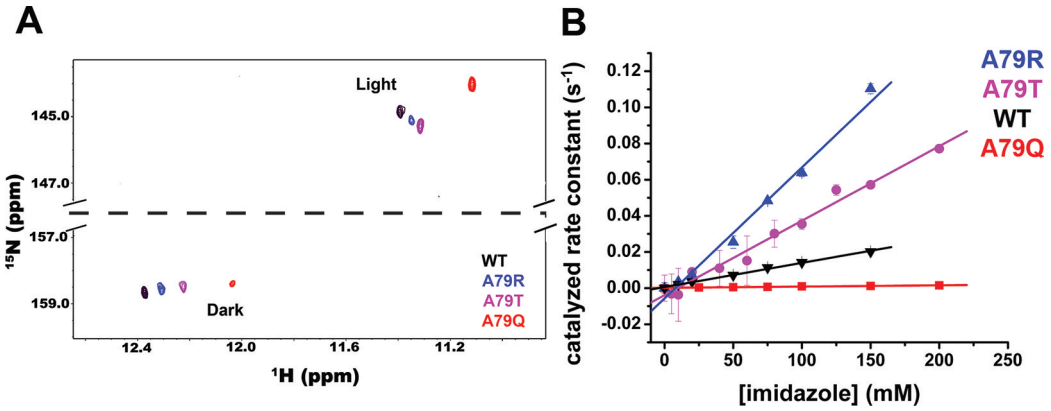

Figure 4. A79 variants depict alteration in N3 H-bonding interactions and susceptibility to base catalysis. (A) The ^{15}N−^{1}H chemical shifts of the N3 position of the flavin isoalloxazine ring are altered by similar magnitudes and in similar directions in both the light and dark states of WT, A79R, and A79T. Notably, the A79Q variant demonstrates larger chemical shift changes. (B) Effect of imidazole on the catalyzed rate constant, showing that the rate of adduct scission in A79Q is very weakly dependent on imidazole compared to WT, consistent with reduced solvent access. In contrast, A79T and A79R show more pronounced solvent access with correspondingly stronger effects of imidazole on rate enhancement.

temperature. Thus, A79 variants capable of H-bonding to O2 seem to stabilize the structural plasticity observed in EL222.

Examination of the temperature-dependent kinetic properties also indicates that the properties of H-bonding to O2 and N1 correlate with the relative energy barriers and the observed kinetics. Not surprisingly, the rapid cycling A79R variant demonstrates the lowest activation barrier (64 kJ/mol) during dark-state recovery, whereas the long-lived A79Q has the highest activation barrier (100 kJ/mol). On the other hand, the rapid cycling A79T variant has an activation barrier (68 kJ/mol) similar to that of WT EL222 (63 kJ/mol). Examination of the relative enthalpic and entropic contribution reveals that A79T has a more favorable entropic contribution (−10 kJ/mol) than the WT (−20 kJ/mol) at 298 K. Similar to A79T, the A79Q variant also exhibits a significantly more favorable entropic contribution (11 kJ/mol at 298 K), although it is not large enough to offset the activation barrier. Thus, H-bonding interactions at N1 and O2 entropically stabilize the light-state adduct.

The origins of the activation energy stabilization could result from changes in solvent accessibility, steric hindrance of active site residues, perturbation of the electronic state of the FMN chromophore, or alterations in the H-bonding network involving the N1, O2, and N3 positions of the flavin ring. To better clarify the mechanism of photocycle perturbation in WT EL222 and A79 variants, we analyzed the proteins for their sensitivity to base catalysis and structural or electronic alteration via NMR analysis.

Effect of the H-Bonding Network and Electronic Stabilization. The N3 position of the flavin ring is protonated in both the dark and light states of LOV proteins and is readily observable in ^{15}N−^{1}H HSQC spectra with characteristic far downfield chemical shifts on both nuclei. Moreover the H atom of N3 is involved in a network of H-bonding interactions involving several protein side chains and the O2 and O4 carbonyls and N1 positions of the flavin ring (Figures 2C−E and 4A). Thus, the N3 proton functions as a probe for alterations of H-bonding interactions at the N1 and O2 positions. Introduction of A79R, A79T, and A79Q mutations results in an upfield shift of the N3 proton (Figure 4A), consistent with increased electron density on the N3 proton and strengthened H-bonding interactions at N1 and O2. This is consistent with weakening of the hydrogen bond between N3 and Asn107 residue, perhaps because of the increase in the strength of H-bonding interactions at the neighboring N1 and O2 positions. Moreover, with the exception of WT EL222 where A79 is incapable of H-bonding to N1 and O2, the degree of chemical shift directly correlates with the change in adduct-state stability.

Importantly, additional alterations of the chemical environment are evident from the relative ^{1}H chemical shifts of the N3-bound proton between the A79 variants in the dark and lit states. Whereas the chemical shift changes resulting from introduction of Thr or Arg residues at the Ala79 position are similar in both states, the A79Q variant has significantly greater upfield shifts in both spectra (Figure 4A). This is consistent with stabilization of additional electron density near N3, altering the electronic environment to stabilize the light-state adduct.

Solvent Accessibility and Rate Catalysis in LOV Domains. Studies of other LOV proteins indicate that solvent access and steric stabilization are primary mediators of adduct scission kinetics.[15−17] While the latter cannot be directly observed experimentally, solvent access can be probed by the ability of imidazole to access the active site and catalyze the recovery process.[15] In the absence of an external base, solvent can catalyze adduct reversion. Greater solvent access should result in a decrease in the relative energy of activation (catalytic activation). Indeed, the active site accessibility has a direct correlation with the energy of activation in the A79 series (Figure 4B). Similarly, the strong H-bonding character of the A79Q variant also results in a more closed active site structure, inhibiting solvent- and imidazole-based catalysis. The A79T and A79R variants exhibit progressively increased kinetic acceleration with imidazole (57- and 100-fold relative to that of A79Q, respectively) that correlates with increases in the activation barrier. Importantly, WT EL222 is 4-fold less susceptible to kinetic acceleration with imidazole than A79T and 7-fold less than A79R variants yet demonstrates an activation barrier identical to that of A79T.

DISCUSSION

Here we demonstrate that a critical aspect of LOV photophysics in EL222, the lifetime of the photoinduced adduct upon dark-state reversion, exhibits unusual non-Arrhenius behavior. This results from increased solvent access and increased flavin

vibrational freedom and potentially involves structural changes between the LOV core and HTH domain. Kinetic and sequence analyses reveal that a key H-bonding residue that is conserved in most LOV proteins contributes to non-Arrhenius behavior and regulates adduct stability. Introduction of the Gln conserved in other LOV proteins significantly reduces the non-Arrhenius dependency and stabilizes the light-state adduct. NMR, base catalysis, and kinetic studies reveal that the H-bonding property of the A79 position is directly correlated with adduct stability, with Gln residues optimally closing off solvent access, while maintaining three H-bonding contacts, (N1, O2, and ribityl O4*) that rigidify LOV structural dynamics.

Non-Arrhenius behavior has been observed in a variety of enzymes, in which increased temperature most commonly induces a less active conformation.[32] Studies of such enzymes demonstrated that the nature of the deviation from a linear temperature dependency may inform on the difference in mechanism between the two temperature regimes.[32,34,35] In these cases, the deviation can display concave or convex curvature[31,35] or sharp transitions between two linear regimes.[32,34] Via application of this background to EL222, it is clear that the hydrogen bonding capabilities of our A79 variants dictate the magnitude and type of non-Arrhenius deviation. The sharp transitions observed in WT, A79R, and A79Q indicate the presence of two distinct conformations that differ in reactivity or mechanism. The minor temperature-dependent changes in CD spectra clearly indicate that any structural changes must be confined to loop regions or involve subtle alteration of H-bonding networks. Position 79 is located in the Eα−Fα loop and anchors the FMN in other LOV domains through H-bonding interactions between the Gln side chain and the N1−O2 and O4* positions. The marked decrease in nonlinear Arrhenius behavior in A79Q variants indicates the importance of this H-bonding locus in maintaining the fidelity of the FMN pocket. Further, the curved transition in A79T variants is reminiscent of non-Arrhenius behavior in PYP, where the photoactivation process is coupled to temperature-dependent partial unfolding.[31] Similarly, a single H-bond to O2 in the EL222 A79T variant stabilizes the LOV core compared to WT; however, this change is insufficient to prevent disruption of Eα−Fα loop contacts with FMN. Rather, increased temperatures result in a gradual transition between the two structural states. Combined, our A79 variants demonstrate a lack of H-bonds to the active site flavin introduces plasticity to the LOV active site and modulates adduct lifetime.

Hydrogen bonding interactions at the N1−O2 locus rigidifies the FMN binding pocket and induces stabilization of the light-state adduct. Previous studies of the LOV protein VVD indicated that the light state can be stabilized via steric and electronic perturbation of the active site flavin, regulation of solvent access to FMN, and alteration of the electron density on the *re* face of the active site flavin.[15] The N1 position adjacent to the surface Eα−Fα loop provides a direct route to affect all three of these mechanisms. Disruption of Gln N1−O4* interactions in WT and A79T variants provides a solvent accessible surface to the active site Cys and FMN moieties. Indeed, imidazole catalysis reflects increased solvent access and a direct correlation between susceptibility to base catalysis and enzyme kinetics. Further, the presence of a positively charged residue near N1 and H-bonding interactions to the N1 position are direct modulators of flavin reduction potentials in flavoenzymes.[36,37] These H-bonds favor flavin reduction and stabilization of N5−sulfite complexes.[36,37] Thus, H-bonding interactions at N1 and O2 in A79Q variants may support regulation of the flavin redox potential in a similar fashion. The stabilization of charge is reflected in alteration of the N1 chemical shift that is altered only in the presence of the A79Q side chain and not A79T.

Coupling modulation of the flavin electronic environment with conformational dynamics of LOV proteins may be a conserved phenotype among LOV domains. In VVD and phototropin, residues on the *re* face of the flavin modulate structural plasticity and adduct stability.[15] In particular, a single Leu → Phe substitution dictates the different properties of LOV1 and LOV2 domains.[20] In EL222, we have shown a different mechanism of altering the electronic properties of the flavin that also modulate structural dynamics. However, similar to VVD, these EL222 variants do not affect the protein signaling mechanism and further expand the role of flavin H-bonding residues in affecting LOV photophysics.

The effect of flavin−pyrimidine ring H-bonding interactions on electronic modulation is supported by recent studies of rate-altering variants of YtvA.[12] There, conserved residues interacting with the O2−N3−O4 locus were analyzed for their effect on triplet formation, adduct formation kinetics, and stabilization of the light-state adduct. Introduction of negatively charged residues destabilized adduct formation and adduct stability, consistent with H-bonding residues stabilizing increased electron density at the N1 position by forming extensive H-bonding networks at the O2−N3−O4 locus. In general, LOV proteins stabilize C4a adducts in a manner analogous to that of flavoenzymes, which are tuned for reduction potential through modulation of the H-bonding character at N1 and positions O2, N3, and O4.

Combined, we have demonstrated a new naturally occurring LOV variant that regulates LOV photocycle kinetics and active site plasticity. Notably, the mechanism of stabilization is similar to those identified in other LOV systems;[15,16] however, the active site variants here modulate adduct stability from 2 to 300 s at the single A79 site but without grossly affecting structure or signaling mechanisms (Figure S1 of the Supporting Information). This begs the question of why this residue is conserved in LOV domains, except for this particular clade of marine bacterial proteins that all have abandoned the conserved Gln to afford greater dynamic flexibility in the LOV active site and increased enzyme kinetics. Notably, the conservation of signaling mechanism with alteration of catalytic turnover makes A79 substitutions ideal for use in optogenetic tools. In addition, detailed kinetic characterization and identification of non-Arrhenius behavior in EL222 facilitate conversion of the light-activated LOV−HTH DNA binding protein into an in vitro tool for regulating gene expression.

■ ASSOCIATED CONTENT

Ⓢ Supporting Information

Temperature dependence of EL222 (14−222) dark-state recovery rates as obtained by mono- or biexponential fitting (Table S1), Arrhenius analyses of EL222 (14−222) dark-state recovery kinetics determined by mono- and biexponential fitting (Figure S1), demonstration of conserved structure and function in A79 variants (Figure S2), SIE data and Eyring analysis of EL222 (14−222) (Figure S3), and Arrhenius analysis of EL222 (14−144) (Figure S4). This material is available free of charge via the Internet at http://pubs.acs.org.

AUTHOR INFORMATION

Corresponding Author

*Department of Biochemistry, University of Texas Southwestern Medical Center, ND8.300, Dallas, TX 75390-8816. Phone: (214) 645-6365. Fax: (214) 645-6353. E-mail: kevin.gardner@utsouthwestern.edu.

Funding

This work was funded by the National Institutes of Health (Grants R01 GM081875 to K.H.G., T32 GM008297 supporting A.I.N., and F32 GM090671 supporting B.D.Z.) and the Robert A. Welch Foundation (Grant I-1424 to K.H.G.).

ABBREVIATIONS

LOV, light, oxygen, voltage; UV, ultraviolet; EPR, electron paramagnetic resonance; FTIR, Fourier transform infrared spectroscopy; H-bond, hydrogen bond; NMR, nuclear magnetic resonance; LIOAS, laser-induced optoacoustic spectroscopy; HTH, helix−turn−helix; SIE, solvent isotope effect; FMN, flavin mononucleotide; PYP, photoactive yellow protein; PAS, period ARNT single-minded domain.

REFERENCES

(1) Chapman, S., Faulkner, C., Kaiserli, E., Garcia-Mata, C., Savenkov, E. I., Roberts, A. G., Oparka, K. J., and Christie, J. M. (2008) The photoreversible fluorescent protein iLOV outperforms GFP as a reporter of plant virus infection. *Proc. Natl. Acad. Sci. U.S.A. 105*, 20038−20043.

(2) Strickland, D., Moffat, K., and Sosnick, T. R. (2008) Light-activated DNA binding in a designed allosteric protein. *Proc. Natl. Acad. Sci. U.S.A. 105*, 10709−10714.

(3) Wu, Y. I., Frey, D., Lungu, O. I., Jaehrig, A., Schlichting, I., Kuhlman, B., and Hahn, K. M. (2009) A genetically encoded photoactivatable Rac controls the motility of living cells. *Nature 461*, 104−108.

(4) Krauss, U., Lee, J., Benkovic, S. J., and Jaeger, K. E. (2010) LOVely enzymes: Towards engineering light-controllable biocatalysts. *Microb. Biotechnol. 3*, 15−23.

(5) Moglich, A., Ayers, R. A., and Moffat, K. (2009) Design and signaling mechanism of light-regulated histidine kinases. *J. Mol. Biol. 385*, 1433−1444.

(6) Zoltowski, B. D., and Gardner, K. H. (2011) Tripping the Light Fantastic: Blue-Light Photoreceptors as Examples of Environmentally Modulated Protein-Protein Interactions. *Biochemistry 50*, 4−16.

(7) Crosson, S., Rajagopal, S., and Moffat, K. (2003) The LOV domain family: Photoresponsive signaling modules coupled to diverse output domains. *Biochemistry 42*, 2−10.

(8) Moglich, A., and Moffat, K. (2007) Structural basis for light-dependent signaling in the dimeric LOV domain of the photosensor YtvA. *J. Mol. Biol. 373*, 112−126.

(9) Zoltowski, B. D., and Crane, B. R. (2008) Light activation of the LOV protein vivid generates a rapidly exchanging dimer. *Biochemistry 47*, 7012−7019.

(10) Zoltowski, B. D., Schwerdtfeger, C., Widom, J., Loros, J. J., Bilwes, A. M., Dunlap, J. C., and Crane, B. R. (2007) Conformational switching in the fungal light sensor Vivid. *Science 316*, 1054−1057.

(11) Harper, S. M., Neil, L. C., and Gardner, K. H. (2003) Structural basis of a phototropin light switch. *Science 301*, 1541−1544.

(12) Raffelberg, S., Mansurova, M., Gartner, W., and Losi, A. (2011) Modulation of the photocycle of a LOV domain photoreceptor by the hydrogen-bonding network. *J. Am. Chem. Soc. 133*, 5346−5356.

(13) Brosi, R., Illarionov, B., Mathes, T., Fischer, M., Joshi, M., Bacher, A., Hegemann, P., Bittl, R., Weber, S., and Schleicher, E. (2010) Hindered rotation of a cofactor methyl group as a probe for protein-cofactor interaction. *J. Am. Chem. Soc. 132*, 8935−8944.

(14) Losi, A., and Gartner, W. (2011) Old chromophores, new photoactivation paradigms, trendy applications: Flavins in blue light-sensing photoreceptors. *Photochem. Photobiol. 87*, 491−510.

(15) Zoltowski, B. D., Vaccaro, B., and Crane, B. R. (2009) Mechanism-based tuning of a LOV domain photoreceptor. *Nat. Chem. Biol. 5*, 827−834.

(16) Christie, J. M., Corchnoy, S. B., Swartz, T. E., Hokenson, M., Han, I. S., Briggs, W. R., and Bogomolni, R. A. (2007) Steric interactions stabilize the signaling state of the LOV2 domain of phototropin 1. *Biochemistry 46*, 9310−9319.

(17) Song, S. H., Freddolino, P. L., Nash, A. I., Carroll, E. C., Schulten, K., Gardner, K. H., and Larsen, D. S. (2011) Modulating LOV domain photodynamics with a residue alteration outside the chromophore binding site. *Biochemistry 50*, 2411−2423.

(18) Nash, A. I., Ko, W. H., Harper, S. M., and Gardner, K. H. (2008) A conserved glutamine plays a central role in LOV domain signal transmission and its duration. *Biochemistry 47*, 13842−13849.

(19) Jentzsch, K., Wirtz, A., Circolone, F., Drepper, T., Losi, A., Gartner, W., Jaeger, K. E., and Krauss, U. (2009) Mutual exchange of kinetic properties by extended mutagenesis in two short LOV domain proteins from *Pseudomonas putida*. *Biochemistry 48*, 10321−10333.

(20) Yamamoto, A., Iwata, T., Tokutomi, S., and Kandori, H. (2008) Role of Phe1010 in light-induced structural changes of the neo1-LOV2 domain of *Adiantum*. *Biochemistry 47*, 922−928.

(21) Kennis, J. T., Crosson, S., Gauden, M., van Stokkum, I. H., Moffat, K., and van Grondelle, R. (2003) Primary reactions of the LOV2 domain of phototropin, a plant blue-light photoreceptor. *Biochemistry 42*, 3385−3392.

(22) Schleicher, E., Kowalczyk, R. M., Kay, C. W., Hegemann, P., Bacher, A., Fischer, M., Bittl, R., Richter, G., and Weber, S. (2004) On the reaction mechanism of adduct formation in LOV domains of the plant blue-light receptor phototropin. *J. Am. Chem. Soc. 126*, 11067−11076.

(23) Alexandre, M. T., Purcell, E. B., van Grondelle, R., Robert, B., Kennis, J. T., and Crosson, S. (2010) Electronic and protein structural dynamics of a photosensory histidine kinase. *Biochemistry 49*, 4752−4759.

(24) Bednarz, T., Losi, A., Gartner, W., Hegemann, P., and Heberle, J. (2004) Functional variations among LOV domains as revealed by FT-IR difference spectroscopy. *Photochem. Photobiol. Sci. 3*, 575−579.

(25) Iwata, T., Nozaki, D., Tokutomi, S., and Kandori, H. (2005) Comparative investigation of the LOV1 and LOV2 domains in *Adiantum* phytochrome3. *Biochemistry 44*, 7427−7434.

(26) Nash, A. I., McNulty, R., Shillito, M. E., Swartz, T. E., Bogomolni, R. A., Luecke, H., and Gardner, K. H. (2011) Structural basis of photosensitivity in a bacterial light-oxygen-voltage/helix-turn-helix (LOV-HTH) DNA-binding protein. *Proc. Natl. Acad. Sci. U.S.A. 108*, 9449−9454.

(27) Blommel, P. G., and Fox, B. G. (2007) A combined approach to improving large-scale production of tobacco etch virus protease. *Protein Expression Purif. 55*, 53−68.

(28) Kay, L. E., Keifer, P., and Saarinen, T. (1992) Pure absorption gradient enhanced heteronuclear single quantum correlation spectroscopy with improved sensitivity. *J. Am. Chem. Soc. 114*, 10663−10665.

(29) Delaglio, F., Grzesiek, S., Vuister, G. W., Zhu, G., Pfeifer, J., and Bax, A. (1995) NMRPipe: A multidimensional spectral processing system based on UNIX pipes. *J. Biomol. NMR 6*, 277−293.

(30) Johnson, B. A., and Blevins, R. A. (1994) NMRView: A computer program for the visualization and analysis of NMR data. *J. Biomol. NMR 4*, 595−740.

(31) Van Brederode, M. E., Hoff, W. D., Van Stokkum, I. H., Groot, M. L., and Hellingwerf, K. J. (1996) Protein folding thermodynamics applied to the photocycle of the photoactive yellow protein. *Biophys. J. 71*, 365−380.

(32) Massey, V., Curti, B., and Ganther, H. (1966) A temperature-dependent conformational change in D-amino acid oxidase and its effect on catalysis. *J. Biol. Chem. 241*, 2347−2357.

(33) Salomon, M., Christie, J. M., Knieb, E., Lempert, U., and Briggs, W. R. (2000) Photochemical and mutational analysis of the FMN-

binding domains of the plant blue light receptor, phototropin. *Biochemistry 39*, 9401−9410.
(34) Han, M. H. (1972) Non-linear Arrhenius plots in temperature-dependent kinetic studies of enzyme reactions. I. Single transition processes. *J. Theor. Biol. 35*, 543−568.
(35) Truhlar, D., and Kohen, A. (2001) Convex Arrhenius plots and their interpretation. *Proc. Natl. Acad. Sci. U.S.A. 98*, 848−851.
(36) Guo, F., Chang, B. H., and Rizzo, C. J. (2002) An N1-hydrogen bonding model for flavin coenzyme. *Bioorg. Med. Chem. Lett. 12*, 151−154.
(37) Ghisla, S., and Massey, V. (1989) Mechanisms of flavoprotein-catalyzed reactions. *Eur. J. Biochem. 181*, 1−17.